COBEM 2023 27TH INTERNATIONAL CONGRESS OF MECHANICAL ENGENEERING

ABCM Brazilian Society of Mechanical Sciences and Engineering
27th ABCM International Congress of Mechanical Engineering
December 04-08, 2023, Florianópolis-SC, Brazil

COB-2023-0308
COMPARATIVE ANALYSIS OF THE STATIC CHARACTERISTICS OF SIMPLIFIED AND FINITE HYDRODYNAMIC JOURNAL BEARING MODELS

Aline de Almeida Soares
Gabriel Alves Marques
Flávio Yukio Watanabe
Mechanical Engineering Department
Federal University of São Carlos
Rod. Washington Luís, km 235 - SP-310
São Carlos - SP - CEP 13565-905
e-mail: alineas@ufscar.br, gabriel.marques@estudante.ufscar.br, fywatanabe@ufscar.br

Abstract. *Hydrodynamic lubrication is a subject of great importance in engineering, and it is essential to the operation of bearings in large hydraulic turbines, reciprocating hermetic compressors and magnetic read heads. The effects of hydrodynamic lubrication were discovered experimentally by Beauchamp Tower in 1883 and mathematically formulated by Osborne Reynolds in 1886, resulting in the theory of hydrodynamic lubrication applied to cylindrical journal bearings, synthesized in a partial differential equation: the Reynolds equation. This equation, derived from the Navier-Stokes and continuity equations applied to the bearing fluid film, describes the behavior of lubricant pressure along the axial and radial/circumferential directions of the bearing, based on dimensional characteristics, operating conditions, and properties of the lubricating fluid, usually characterized by the Sommerfeld number, a dimensionless parameter used in hydrodynamic lubrication analysis. The analytical solution of the Reynolds equation is only possible if some simplifications of the differential equation are adopted and resulting in the infinitely long bearing and short bearing models. The whole Reynolds equation can be solved by applying numerical approaches such as Finite Difference Method (FDM), Finite Volume Method (FVM) and Finite Element Method (FEM), generating finite bearing models. Although limited, the simplified models results are close to the complete solution for some geometric configurations and specific operation conditions. Additionally, in the radial clearance divergence field, mathematical or numerical solutions result in negative hydrodynamic pressures in the fluid film, which does not actually occur, since there is a rupture of the fluid film often characterized as a kind of cavitation phenomenon. In this way, different boundary conditions make it possible to obtain feasible results such as Gümbel, Reynolds/Swift-Stieber and Jakobsson-Floberg-Olsson (JFO) boundary conditions. Although the literature on the subject presented is wide, there is a gap in the direct comparison between simplified and finite models of hydrodynamic journal bearings. Therefore, the main objective of this study is to present this comparative analysis, considering characteristic results such as pressure profile in the fluid film, locus of the rotor center position and bearing load capacity. The differences and similarities between different models are evidenced providing an understanding of the limits of use of the results obtained from the simplified models of hydrodynamic journal bearings. In general, for small rotor eccentricities, if the bearing width/diameter ratio, (L/D), is smaller than 1, the short bearing model may be used, and if L/D is bigger than 1, the infinitely long bearing model may be useful. Furthermore, journal bearings operating with eccentricity bigger than half the bearing radial clearance, independently of their aspect radio, L/D, it is recommended the use a finite bearing numerical solution.*

Keywords: *hydrodynamic lubrication, Reynolds equation, boundary conditions, analytical solution, Finite Difference Method.*

1. INTRODUCTION

The hydrodynamic lubrication phenomenon occurs when non-parallel rigid bearing surfaces lubricated by a film-fluid slide over each other, forming a converging wedge of fluid and forming a lifting pressure (Williams, 1994), and plays an important role in industry tribology, being essential to the operation of bearings in large hydraulic turbines, or small reciprocating hermetic compressors and magnetic read heads.

Historically, the discovery and formulation of hydrodynamic lubrication mechanism are attributed to three researchers: Nikolai P. Petrov (1836-1920), Beauchamp Tower (1845-1904) and Osborne Reynolds (1842-1912). Within a few years (1883-1886) and independent of each other, they laid the foundations of this engineering science branch. In common, all three perceived that the lubrication process is due not to the mechanical interaction of two solid surfaces but to the dynamics of a fluid film separating them (Pinkus, 1987).

The main interest of Petrov was in the fluid friction area and, in 1833, he proposed the hydrodynamic nature of friction in sliding bearings but did not extend his insight into the nature of friction to the load carrying capacity of bearings (Pinkus, 1987). In the same year 1883, the essence of hydrodynamic lubrication and the associate load capacity was first clarified experimentally by Tower in a test rig with partial sliding bearing. Based on Tower's experiments, Reynolds formulated a theory of hydrodynamic lubrication in 1886 and, since then, Reynolds' theory allows the development of other theories like elastohydrodynamic, thermohydrodynamic and turbulent hydrodynamic lubrication (Hori, 2006).

Reynolds lubrication theory considers a thin fluid film between two solid surfaces and applying the Navier-Stokes and continuity equations to the fluid, the Reynolds' equation is obtained. This equation is a partial differential equation that describes the hydrodynamic pressure generated in a fluid film when the surfaces undergo relative motion, and its full analytical solution is not possible. Simplified models, like infinitely long bearing and short bearing, allows obtaining reduced analytical solutions, but the full Reynolds equation only may be solved by applying numerical method approaches (Hori, 2006).

Someya (1988) edited the Journal-Bearing Databook in which the static and dynamic characteristics of different types of hydrodynamic bearings in use are established and organized, combining results obtained by means of numerical calculations and measured on different test rigs.

Most journal bearings, in the past, had width bigger than twice de diameter, but in recent years, short bearings are being used aiming the reduction of friction loss due to shaft misalignment. Hori (2006) indicates that, nowadays, a typical range of bearing width/diameter ratio, L/D, is 0.5 to 1. At the same time, Norton (2013) indicates that journal bearing range of width/diameter ratio, L/D, is from 0.25 to 2. Furthermore, Harnoy (2003) points out that most journal bearings operate under steady conditions with eccentricity ratios from $\varepsilon = 0.6$ to $\varepsilon = 0.8$, in such a way that the minimum film thickness will be higher than surface asperities or the amplitude of journal vibrations during operation.

Although there is a wide literature on hydrodynamic lubrication subject, there is a gap in the direct comparison between simplified and finite models of hydrodynamic journal bearings. The main objective of this study is to present this comparative analysis, considering characteristic results such as pressure profile in the fluid film and load capacity, as a function of physical and operating characteristics of the bearing.

2. HYDRODYNAMIC JOURNAL BEARING

Hydrodynamic bearings that support rotating shafts by a sliding motion can be classified, according to the direction of load, as radial or axial type, or to the main geometric characteristics, as cylindrical, lobed, partial arc, circular disc, conical, spherical, fixed surface or tilting pad type (Someya, 1989). Hydrodynamic bearings with radial load capacity are generally called journal bearings and a cylindrical journal bearing with plain and fixed surface, as illustrated in Fig. 1, is analyzed in this study, assuming a fixed bearing and rotating shaft.

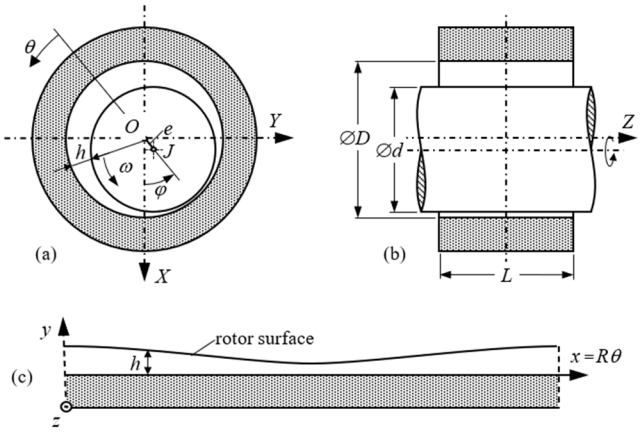

Figure 1. Cylindrical hydrodynamic journal bearing.

where:

- X, Y and Z are inertial cartesian coordinates, x, y and z are local cartesian coordinates;
- θ is angular auxiliar coordinate, being $x = R\theta$
- O and J are bearing and rotor centers, respectively
- d is rotor diameter and D, R and L are bearing diameter, radius and width, respectively
- h is the fluid film thickness ($h = c + e\cos\theta$)
- c is nominal radial clearance ($c = R - r$)
- e and φ are rotor eccentricity and attitude angle in equilibrium position
- ω is rotor angular velocity.

2.1 Reynolds equation

The behavior of lubricant pressure, $p(x,z)$, developed in the fluid film of the cylindrical journal bearing is described by Reynolds equation, expressed in Eq. (1) as a partial differential equation stated in x and z coordinates, related to tangential/circumferential and axial directions, respectively.

$$\frac{\partial}{\partial x}\left(h^3\frac{\partial p}{\partial x}\right)+\frac{\partial}{\partial z}\left(h^3\frac{\partial p}{\partial z}\right)=6\mu U\frac{\partial h}{\partial x}, \tag{1}$$

where, μ is fluid absolute or dynamic viscosity, U is rotor tangential velocity ($U=\omega R$), and $h=h(x)$ for parallel bearing and rotor axis.

Hori (2006) points out that a general solution of Eq. (1) cannot be obtained analytically, and that the following approximated analytical solutions are usually employed:

- The *infinitely long approximation*, proposed by Sommerfeld in 1904, assumes a sufficiently long bearing in the axial direction ($L \gg D$) and neglects the pressure gradient in axial direction ($\partial p/\partial z \approx 0$) of the Reynolds equation, resulting in the simplified Eq. (2).

$$\frac{\partial}{\partial x}\left(h^3\frac{\partial p}{\partial x}\right)=6\mu U\frac{\partial h}{\partial x}, \tag{2}$$

- The *short bearing approximation*, presented by Dubois and Ocvirk in 1953, assumes a sufficiently short bearing in the axial direction ($L < D$) and that the pressure gradient in the axial direction is much larger than that in the circumferential direction ($\partial p/\partial z > \partial p/\partial x$), so that, the pressure gradient in circumferential direction may be neglected in Reynolds equation ($\partial p/\partial x \approx 0$), resulting in Eq. (3).

$$\frac{\partial}{\partial z}\left(h^3\frac{\partial p}{\partial z}\right)=6\mu U\frac{\partial h}{\partial x}, \tag{3}$$

Furthermore, Hori (2006) indicates that for *finite length bearings*, the full two-dimensional Reynolds equation may be solved numerically, for example, by Finite Difference Method (FDM), Finite Volume Method (FVM) and Finite Element Method (FEM). According to Gropper et al. (2016), the FDM is most applied due to its easy implementation, followed by FEM and FVM. Some examples of FDM application are shown by Dwivedi et al. (2013) in hybrid (hydrostatic/hydrodynamic) journal bearing analysis and by Kango et al. (2012) in a numerical investigation of hydrodynamic journal bearing with textured surface.

2.2 Boundary conditions for the fluid film

Analytical or numerical solutions of Reynolds equation require the definition of suitable boundary conditions. In a journal bearing the boundary condition at an axial/lateral end is simply that the fluid film pressure equals to atmospheric pressure (p_0), but in the circumferential direction the fluid film is subjected to rupture in the bearing divergent region growing ($\pi < \theta < 2\pi$), where the clearance is growing, and the inflow of air may occur due to theoretical negative fluid pressure in this region (Hori, 2006). The complexity of this phenomenon led to the adoption of three simplified boundary conditions for the fluid film pressure in circumferential direction, illustrated in Fig. 2 for an infinite length bearing (Someya, 1988).

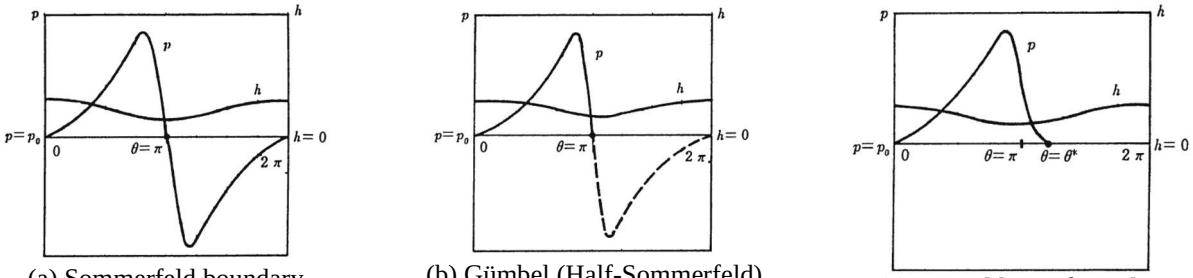

(a) Sommerfeld boundary condition

(b) Gümbel (Half-Sommerfeld) boundary condition

(c) Reynolds/Swift-Stieber boundary condition

Figure 2. Circumferential pressure boundary conditions for cylindrical journal bearing.

Sommerfeld boundary condition (Fig. 2a) assumes that negative fluid pressure occurs in the bearing region with growing clearance ($\pi < \theta < 2\pi$) without fluid film rupture and that fluid pressure $p = p_0$ at $\theta = 0$ and $\theta = \pi$. This boundary condition is seldom applied, except when the bearing pressure is low.

For Gümbel (or Half-Sommerfeld) boundary condition (Fig. 2b), only the positive fluid pressure is considered, and the negative pressure is replaced by atmospheric pressure. Although its simplicity, this condition is physically inappropriate, because the flow and pressure continuity are not satisfied at $\theta = \pi$.

Swift-Stieber or Reynolds boundary condition assumes that both the fluid pressure and pressure gradient are zero, simultaneously, at $\theta = \theta^*$, eliminating the discontinuity problem of Gümbel's condition at $\theta = \pi$, but an interactive procedure must be adopted to determine $\theta *$ along circumferential and axial directions.

The phenomenon of fluid film rupture in bearing divergent region, known as *gaseous cavitation*, usually results in finger-shaped voids and is described by Jakobsson-Flober-Olsson (JFO) theory (Braun and Hannon, 2010). The JFO theory considers the oil film divided into two regions: one region with complete film formation obeys the classic Reynolds equation; another region where the rupture of the oil film occurs. In this second region, only part of the gap is filled with oil and the pressure is considered constant. The JFO boundary condition results from the application of mass conservation in the full-film interface and cavitation zones (Elrod, 1981).

2.3 Load capacity and equilibrium position

Assuming a static vertical load, F, actuating in the rotor shown in Fig. 3, the fluid film hydrodynamic pressure, p, developed in journal bearing supports this load and the rotor equilibrium position is defined by its eccentricity, e, and attitude angle, φ. The fluid film pressure, p, may be integrated to determine the bearing load capacity, W, and its two orthogonal components, W_x and W_y (Harnoy, 2003)

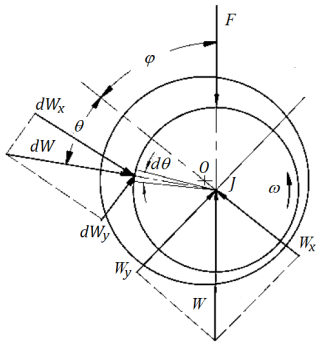

Figure 3. Hydrodynamic bearing load capacity.

The direction of W_x is along bearing and rotor center line (O-J), inclined from the vertical direction by φ, and W_y direction is normal to the W_x. Load capacity components W_x and W_y may be determined integrating the elementary force dW resulting from fluid pressure, p, actuating in an elementary area $dA = Rd\theta dz$, in all bearing surface ($0 < \theta < 2\pi$ and $-L/2 < z < L/2$), resulting in Eq. (4) and (5), respectively.

$$W_x = -\int_0^{2\pi}\int_{-L/2}^{L/2} p\cos\theta \; R \; d\theta \; dz, \tag{4}$$

$$W_y = \int_0^{2\pi}\int_{-L/2}^{L/2} p\,\mathrm{sen}\theta \; R \; d\theta \; dz, \tag{5}$$

The total load capacity of the journal bearing, W, and corresponding attitude angle, φ, are obtained from load capacity components, as shown in Eq. (6) and (7), respectively.

$$W = \sqrt{W_x^2 + W_y^2}, \tag{6}$$

$$\tan\varphi = W_y/W_x, \tag{7}$$

2.4 Infinitely long bearing

In an infinitely long bearing model ($L \gg D$), the solution of simplified Reynolds equation, Eq. (2), allows determining the fluid film hydrodynamic pressure distribution, p, expressed in Eq. (8) for Gümbel boundary condition (Hori, 2006).

The fluid pressure varies only in circumferential (θ) direction, once the pressure gradient in axial direction, $\partial p/\partial z$, was neglected.

$$p(\theta) = \frac{6\mu UR}{c^2}\frac{\varepsilon(2+\varepsilon\cos\theta)sen\theta}{(2+\varepsilon^2)(1+\varepsilon\cos\theta)^2} \qquad (0<\theta<\pi), \tag{8}$$

where, $\varepsilon = e/c$ is the eccentricity ratio ($0 < \varepsilon < 1$).

Considering Eq. (8) and applying in Eq. (4) to (7), bearing load capacity, W, and attitude angle, φ, are determined and expressed in Eq. (9) and (10), respectively (Hori, 2006).

$$W = \frac{6\mu UR^2L}{c^2}\frac{\varepsilon\{4\varepsilon^2+\pi^2(1-\varepsilon^2)\}^{1/2}}{(2+\varepsilon^2)(1-\varepsilon^2)}, \tag{9}$$

$$\tan\varphi = \frac{\pi(1-\varepsilon^2)^{1/2}}{2\varepsilon}, \tag{10}$$

2.5 Short bearing

In a short bearing model ($L < D$), the solution of Eq. (3) results in the fluid film hydrodynamic pressure distribution, p, expressed in Eq. (11) (Hori, 2006). In this case, fluid pressure varies in circumferential (θ) and axial (z) directions, and due to Gümbel boundary condition, only positive pressures are considered.

$$p(\theta,z) = \frac{3\mu U}{Rc^2}\left(\frac{L^2}{4}-z^2\right)\frac{\varepsilon\text{sen}\theta}{(1+\varepsilon\cos\theta)^3} \qquad (0<\theta<\pi \text{ and } -L/2<z<L/2) \tag{11}$$

Applying Eq. (11) in Eq. (4) to (7), bearing load capacity, W, and attitude angle, φ, are determined and expressed in Eq. (9) and (10), respectively (Hori, 2006).

$$W = \frac{\mu UL^3}{4c^2}\frac{\varepsilon}{(1-\varepsilon^2)^2}[\pi^2(1-\varepsilon^2)+16\varepsilon^2]^{1/2}, \tag{12}$$

$$\tan\varphi = \frac{\pi}{4}\frac{(1-\varepsilon^2)^{1/2}}{\varepsilon}, \tag{13}$$

2.6 Finite bearing

Finite length bearings are also considered in this study and a computational algorithm was developed, based on Finite Difference Method (FDM) and Gümbel boundary condition for fluid pressure. In this method, the plain bearing surface is discretized in a grid pattern with nodal points in circumferential (x) and axial directions (z), as illustrated in Fig. 4.

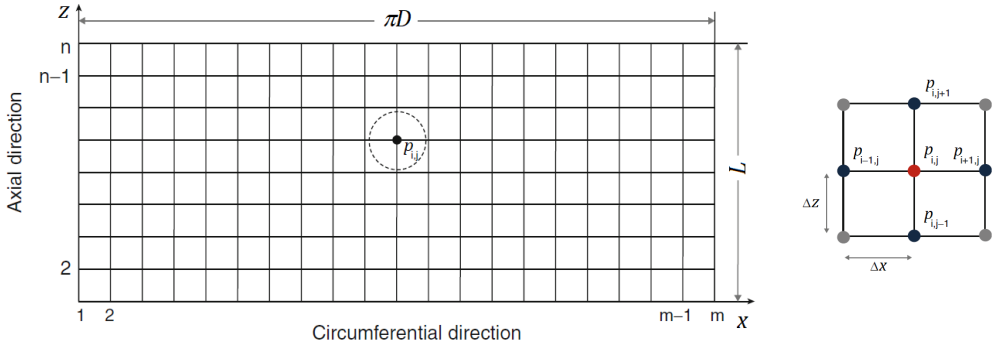

Figure 4. Grid pattern in plain bearing surface (Dmochowski et al., 2013).

The derivatives in bidimensional Reynolds equation, Eq. (1), a partial differential equation, are approximated to finite differences of pressure and fluid film thickness of the nodal points, based on Taylor expansion of a continuous and

differentiable function at (i, j) neighboring points, and considering the central difference approximations, resulting in the set of Eq. (14).

$$\begin{cases} \dfrac{\partial p}{\partial x} \cong \dfrac{p_{i+1,j} - p_{i-1,j}}{2\Delta x} \\ \dfrac{\partial^2 p}{\partial x^2} \cong \dfrac{p_{i+1,j} - 2p_{i,j} + p_{i-1,j}}{\Delta x^2} \\ \dfrac{\partial p}{\partial z} \cong \dfrac{p_{i,j+1} - p_{i,j-1}}{2\Delta z} \\ \dfrac{\partial^2 p}{\partial x^2} \cong \dfrac{p_{i,j+1} - 2p_{i,j} + p_{i,j-1}}{\Delta z^2} \end{cases} \tag{14}$$

The pressure at the nodal point (i, j) can be expressed by Eq. (15):

$$p_{i,j} = a_0 + a_1 p_{i+1,j} + a_2 p_{i-1,j} + a_3 p_{i,j+1} + a_4 p_{i,j-1}, \qquad (i = 1, 2, \dots, m-1;\ j = 1, 2, \dots, n-1) \tag{15}$$

where $p_{i,j}$ is the pressure at the nodal point (i, j) and a_0, a_1, a_2, a_3 and a_4 are constants defined the respective nodal point.

Applying the boundary conditions, both in the circumferential and axial directions, the obtained set of (m x n) algebraic equations can be solved by numerical methods.

The computational algorithm, developed in Matlab software, applying the FDM and the Gümbel boundary condition in an interactive way, allowing the determination of fluid film pressure, rotor center equilibrium position and load capacity, for different journal bearing geometric configurations and operation conditions. The flowchart of Figure 5 shows the procedure adopted for obtaining the journal bearing static characteristics.

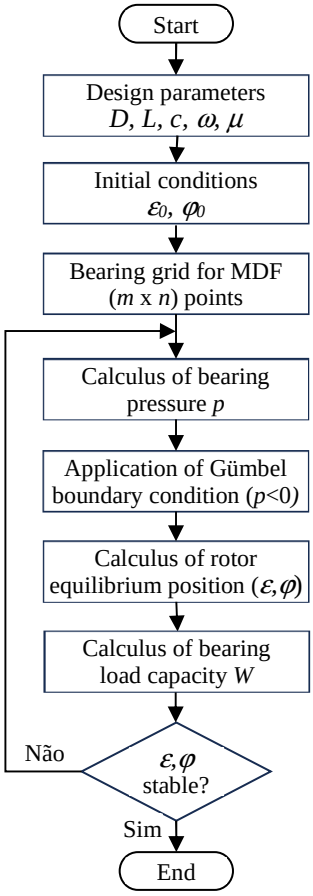

Figure 5. Procedure for calculation of static characteristics of journal bearing.

3. RESULTS AND DISCUSSION

Hydrodynamic journal bearing static characteristics, like fluid film pressure, rotor equilibrium position and load capacity were determined for the three different bearing models: infinitely long, short and finite bearing, assuming in all three cases, a bearing width/diameter ratio $L/D = 1$ and a eccentricity ratio $\varepsilon = 0.7$.

Figure 6 illustrates the fluid film dimensionless pressure ($p^* = p\,(c/R)^2/6\mu\omega$) distribution in each one of these bearing models and assuming a Gümbel boundary condition for negative pressures.

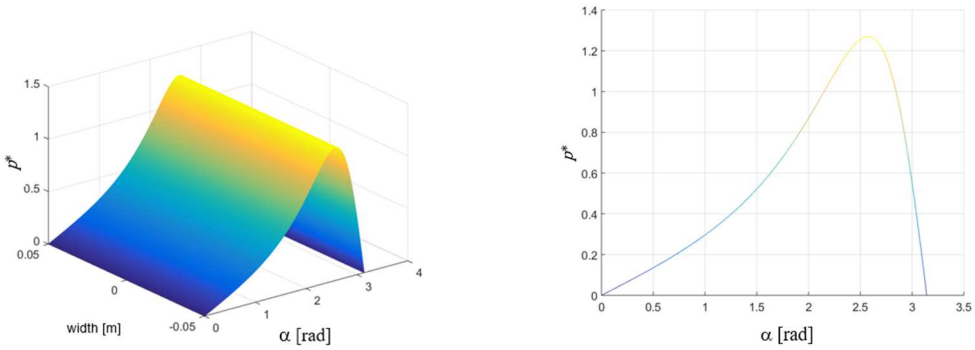

(a) Infinitely long bearing (3D and side view plotting)

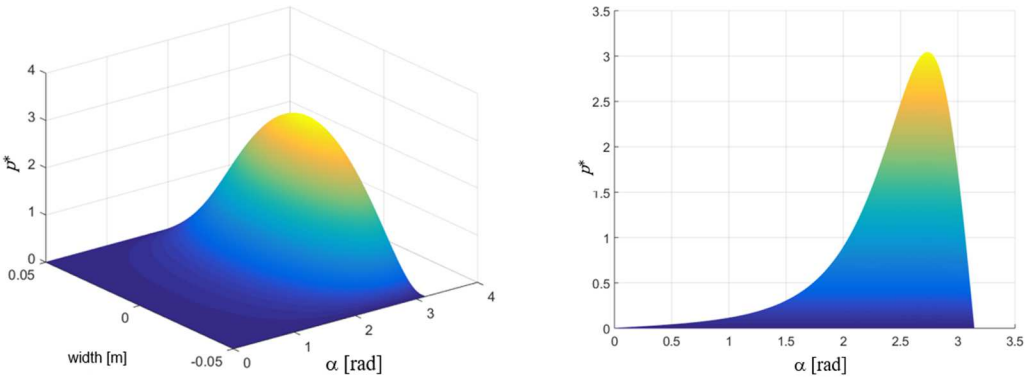

(b) Short bearing (3D and side view plotting)

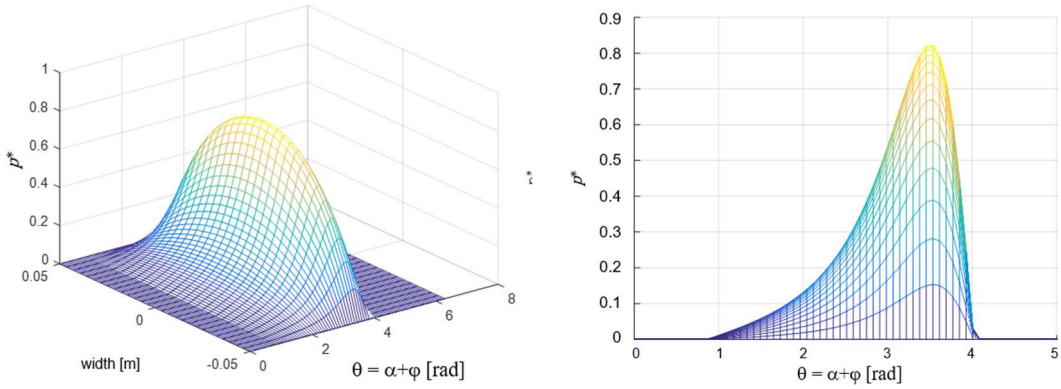

(c) Finite bearing (3D and side view plotting)

Figure 6. Fluid film dimensionless pressure in hydrodynamic journal bearings.

As explained before, it can be noted that in an infinitely long bearing (Fig. 6a), fluid pressure varies only in circumferential direction, once the pressure gradient $\partial p/\partial z$ was neglected in this simplified bearing solution. For the short bearing model (Fig. 6b), fluid pressure varies in circumferential and axial direction, even with the pressure gradient in circumferential direction $\partial p/\partial x$ neglected, because film thickness varies along this direction. The film pressure in a finite bearing is illustrated in Fig. 6c and one can note that fluid pressure varies in both directions, circumferential and axial, in a similar way of short bearing, but with different pressure levels.

The locus of rotor center under static equilibrium position, defined by the combination of eccentricity ratio ε and the attitude angle φ of rotor-bearing system, are shown in Fig. 7a for infinitely long and short bearing. One can note that, as shown in Eq. (7) and Eq. (10), the rotor center locus for both cases are not influenced by L/D ratio. For finite bearings (Fig. 7b), the L/D ratio influences rotor static equilibrium position and, for lower values of L/D the locus of rotor center approaches the short bearing locus, as well for higher values of L/D the locus of rotor center approaches the infinitely long bearing locus.

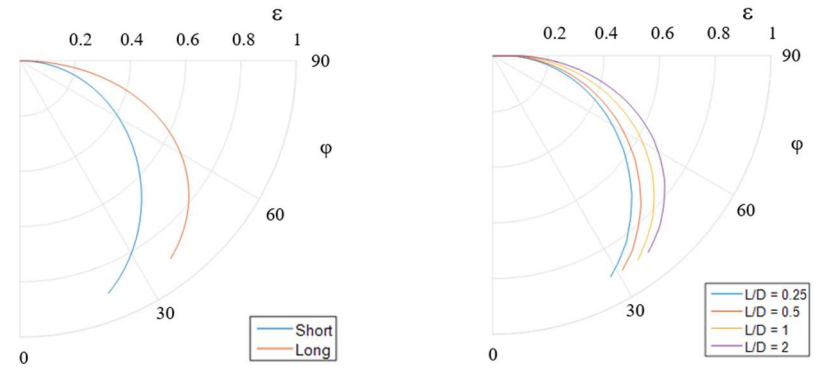

(a) Short and infinitely long bearings (b) Finite bearing

Figure 7. Locus of the rotor center under Gümbel's condition.

The bearing dimensionless load capacity ($W^* = W/(3\mu\omega R^3 L/c^2)$) may be determined for the three bearing models and the results are exemplified in Fig. 8 as a function of eccentricity ratio, ε, and for different aspect ratios L/D.

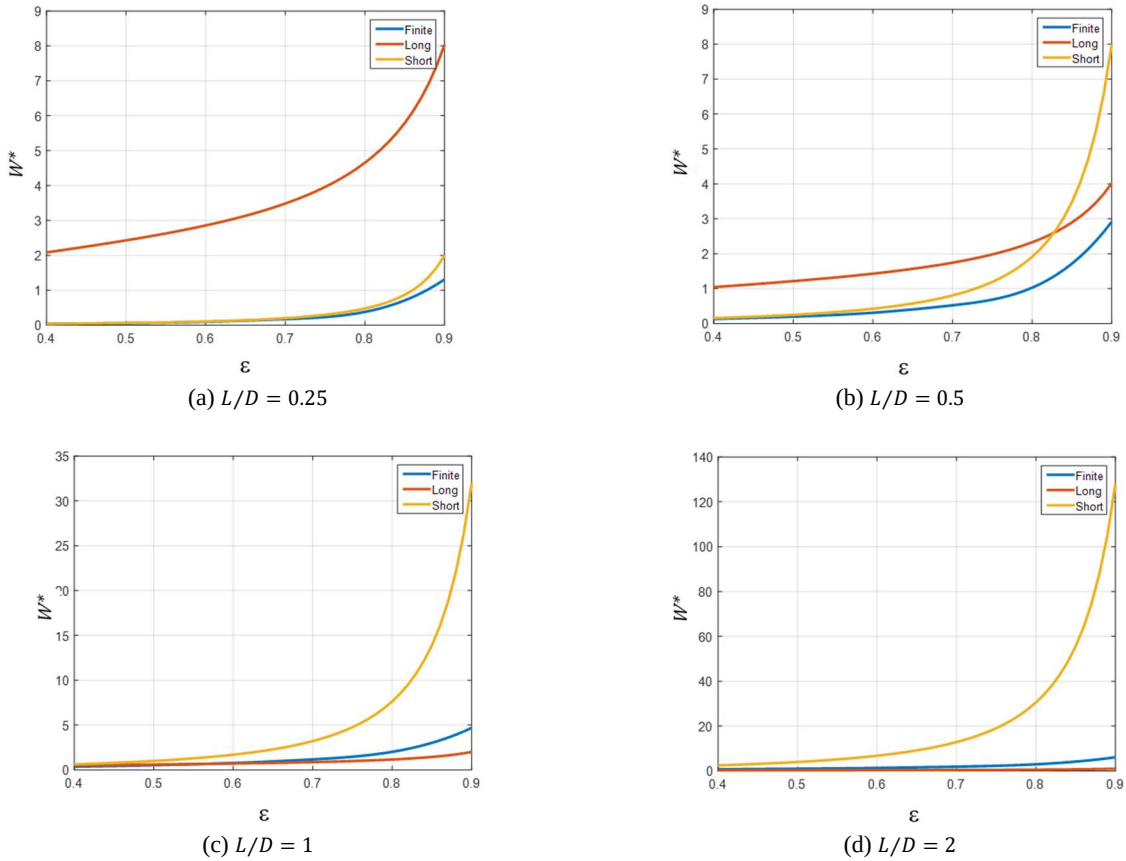

(a) $L/D = 0.25$ (b) $L/D = 0.5$

(c) $L/D = 1$ (d) $L/D = 2$

Figure 8. Load capacity x eccentricity ratio for different journal bearing models.

In a hydrodynamic journal bearing with small width, $L/D = 0.25$ (Fig. 7a), the dimensionless load capacities W^* of short and finite bearings models are practically coincident, especially for eccentricity ratio $\varepsilon < 0.7$, and both are smaller

than the fictitious load capacity of the infinitely long bearing. A similar behavior occurs when $L/D = 0.5$ (Fig. 7b), but for eccentricity ratio $\varepsilon < 0.5$. Furthermore, for $L/D = 0.5$ and $\varepsilon > 0.7$, the W^* of short bearing increases abruptly, overcoming W^* of infinitely long bearing model. The dimensionless load capacities W^* of infinitely long and finite bearings with aspect radio $L/D = 1$ (Fig. 7c) and $L/D = 2$ (Fig. 7d) are very close to each other, especially for $\varepsilon < 0.7$, and both are smaller than W^* of short bearing model, mainly for $\varepsilon > 0.6$.

Although finite bearing results are being used as a reference, it is important to note that this is an approximate numerical solution, but the comparison with the other bearing models allows highlighting the limitations of each analytical model.

4. CONCLUSIONS

Hydrodynamic journal bearings are widely used in industry and the suitable design of this machine element may provide a long life for industrial and domestic equipment. For this purpose, commercial software and standards with design procedure are employed. All these procedures are based on the fluid film Reynolds equation solution and different approaches may be adopted. Usually, a journal bearing aspect ratio, L/D, may varies from 0.25 to 2, but nowadays a more typical range of L/D is 0.5 to 1. Long bearings support heavy loads, but the shaft misalignment may lead to scraping problem in bearing sides. This problem may be minimized if short bearings are adopted, but with the consequent loss of carrying capacity.

In this study, a comparation between infinitely long, short and finite journal bearing models was performed and the similarities, discrepancies and limitations on fluid hydrodynamic pressure and load capacity were pointed out. In general, for small eccentricity ratio ($\varepsilon < 0.5$), if the bearing aspect radio, L/D, is smaller than 1, the short bearing model may be used, and if L/D is bigger than 1, the infinitely long bearing model may be useful. Furthermore, journal bearings operate with eccentricity ratio $\varepsilon > 0.5$, usually 0.6 to 0.8, therefore it is recommended the use a finite bearing numerical solution, independently of their aspect radio, L/D.

5. REFERENCES

Braun, M.J., Hannon, W.M., 2010. “Cavitation formation and modelling for fluid film bearings: a review”. *Journal of Engineering Tribology*, Vol. 224, No. 9, pp. 839-863.

Dmochowski, W.M., Dadouche, A. and Fillon, M., 2013. *Finite Difference Method for Fluid-Film Bearings*, in: Wang, Q. J. and Chung Y.-W. (Ed.) *Encyclopedia of Tribology*, Springer, New York.

Dwivedi, V.K., Chand, S. and Pandey, K. N., 2013. “Effect of number and size of recess on the performance of hybrid (hydrostatic/hydrodynamic) journal bearing”, *Procedia Engineering*. Vol. 51, pp. 810-817.

Elrod, H.G., 1981. “A Cavitation Algorithm”. *Journal of Lubrication Technology*, Vol. 103, No. 3, pp. 350-354.

Gropper, D., Wang, L. and Harvey, T.J., 2016. “Hydrodynamic lubrication of textured surfaces: A review of modeling techniques *and* key findings”. *Tribology International*, Vol. 94, pp. 509-529.

Harnoy, A., 2003. *Bearing design in machinery*. Marcell Dekker.

Hori, Y., 2006. *Hydrodynamic lubrication*. Springer, Tokyo.

Kango, S., Singh, D. and Sharma, R.K., 2012. “Numerical investigation on the influence of surface texture on the performance of hydrodynamic journal bearing”, Vol. 47, pp. 469-482.

Norton, R.L., 2011. *Machine Design: An Integrated Approach*. Prentice Hall, 4th ed. New Jersey.

Pinkus, O., 1987. “The Reynolds Centennial: A Brief History of the Theory of Hydrodynamic Lubrication”, *Transaction of the ASME - Journal of Tribology*, Vol. 109, pp. 2-15.

Someya, T., 1988. *Journal-bearing databook*. Springer-Verlag, Berlin.

6. RESPONSIBILITY NOTICE

The authors are the only responsible for the printed material included in this paper.